Unearthing the Real-Time Excited State Dynamics from Antenna to Rare Earth Ions Using Ultrafast Transient Absorption

Waygen Thor, Hei-Yui Kai, Yik-Hoi Yeung, Yue Wu, Tsz-Lam Cheung, Leo K B Tam, Yonghong Zhang, Loïc J Charbonnière, Peter A Tanner, Ka-Leung Wong

JACS Au
AN OPEN ACCESS JOURNAL OF THE AMERICAN CHEMICAL SOCIETY

pubs.acs.org/jacsau
Article

Unearthing the Real-Time Excited State Dynamics from Antenna to Rare Earth Ions Using Ultrafast Transient Absorption

Waygen Thor, Hei-Yui Kai, Yik-Hoi Yeung, Yue Wu, Tsz-Lam Cheung, Leo K. B. Tam, Yonghong Zhang, Loïc J. Charbonnière,* Peter A. Tanner,* and Ka-Leung Wong*

Cite This: JACS Au 2024, 4, 3813−3822

ABSTRACT: The conventional energy transfer pathway in organic lanthanide complexes is purported to be from the excited singlet state of the chromophore to the triplet state and subsequently directly to the emitting state of the trivalent lanthanide ion. In this work, we found that the energy transfer occurs from the triplet state to the nearest energy level, instead of directly to the emitting state of the lanthanide ion. The triplet decay rate for different lanthanide ions follows an energy gap law from the triplet level to the receiving level of the lanthanide ion. Three different categories of complexes were synthesized and inspected using different techniques, demonstrating the universality of our findings. This work renews the insights to conventional findings, highlighting the importance of the energy gap between the triplet state and the nearest lanthanide energy level in optimization of light harvesting. The rationale of ligand design of chromophores should be reconsidered, leading to various applications of lanthanide complexes with enhanced quantum yield and brightness.

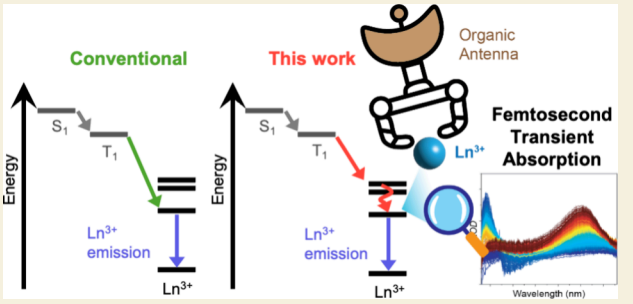

KEYWORDS: *Lanthanide luminescence, Excited state dynamics, Photosensitization mechanism, Time-resolved spectroscopy, Energy transfer, Transient absorption*

INTRODUCTION

In 1942, Weissman demonstrated strong Eu^{3+} luminescence from organic coordinated complexes, and this method of harvesting light from organic chromophores is widely recognized as the antenna effect.[1] With the aid of the antenna effect, luminescence from trivalent lanthanide ions can be harvested despite the weak absorption coefficient of Ln^{3+}.[2,3] This discovery expands the possibilities of applying organic lanthanide complexes in various fields of application, including bioimaging,[4−6] up-conversion,[7−9] and functional materials.[10−12] Understanding the energy transfer (ET) mechanism is crucial for optimizing the optical properties of organic lanthanide complexes. The nonradiative processes from the organic chromophore to the Ln^{3+} are typically responsible for determining the quantum yield[13] or brightness[14] of a chemical system. This ET from the antenna is generally said to follow the sensitization pathway from singlet (S_1) → triplet (T_1) → Ln^{3+} (Figure 1a).[15−19] Often, the optimization of the ligand focuses upon the transfer from the triplet state to the lanthanide ion.[20,21] However, the energy can also be transferred directly to the lanthanide singlet state,[22] or from charge transfer (CT) states, which form electronically conjugated donors and acceptors in the same system.[23,24] The main focus herein is on the conventional decay pathway from S_1 to T_1 and subsequently to Ln^{3+} since there is no spectral evidence that CT states are involved in the systems investigated in this work, and we do not discuss this further.[25]

Gaining mechanistic understanding of lanthanide luminescence is challenging, and each ET step is crucial, including the intersystem crossing (ISC) from $S_1 \rightsquigarrow T_1$. It has been argued that the ISC rate is the rate-determining step to sensitize the luminescence of Ln^{3+}.[26,27] Despite the fact that ISC from $S_1 \rightsquigarrow T_1$ is spin-forbidden to first order, the mixing of singlet and triplet states is facilitated by a nearby heavy atom.[28] The efficiency of ISC plays an important role in the ET model, as proven by calculation and experiment. Arppe et al. reported that an enhanced ISC rate can lead to the faster depopulation rate of the triplet state, including phosphorescence rate and ET rate to the lanthanide ion.[29] Similar phenomena demonstrating the importance of ISC have been observed in the case of a Tb-coordinated complex using a multiconfigurational calculation.[30] Introducing a Ag^+ or Cu^+ metal cation into a Tb-coordinated peptide loop decreases the rise time of Tb^{3+} due to the enhanced ISC by the heavy atom effect.[31] By

Received: June 3, 2024
Revised: July 4, 2024
Accepted: July 5, 2024
Published: August 20, 2024

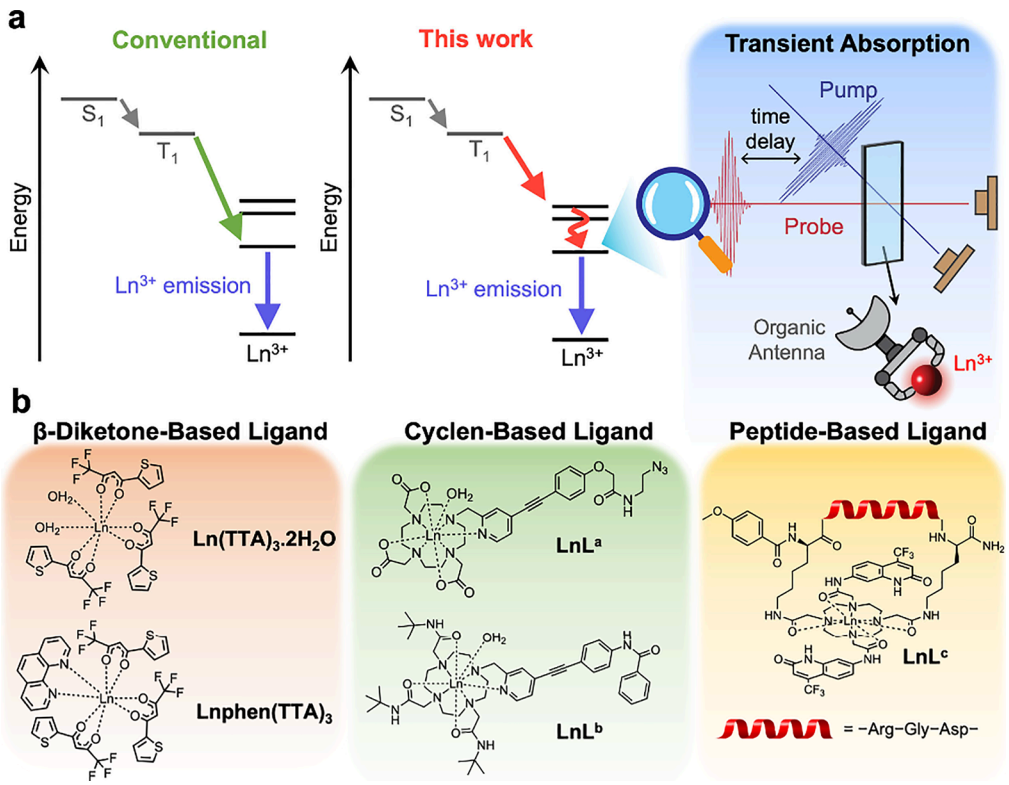

Figure 1. (a) Illustration of the Jablonski diagram showing the conventional ET mechanism and the proposed ET mechanism occurring from the triplet state to the nearest energy state, as investigated in this work, instead of directly to the luminescence state of the trivalent lanthanide ions. This process can be monitored by employing femtosecond transient absorption spectroscopy, which monitors the change in the absorption at different time delay as illustrated. (b) The chemical structures of **Ln(TTA)$_3$·2H$_2$O**, **Lnphen(TTA)$_3$**, **LnL^a**, **LnL^b**, and **LnL^c**, which can be categorized into *β*-diketone-based, cyclen-based, and peptide-based ligands, to demonstrate the universality of the proposed mechanism.

incorporating a heavier atom in the meta position of 1-phenyl-3-pyridin-3-yl-propane-1,3-dione (PPPD) and investigating the system using modeling, Wu et al. found that the ligand-centered ISC rate increased, followed by the rise rate of the $^5D_0 \rightarrow {}^7F_2$ emission. In addition, a model with a good spin quantum number of the combined metal−ligand system was introduced to gain insight into the underlying ET.[19]

The role of ISC is more significant in the case of nonluminescent lanthanide complexes, where ligand-centered transitions are solely observed. Tobita et al.[32] reported that phosphorescence lifetimes were found to be similar for closed shell La^{3+} (0.13 s) and Lu^{3+} (0.12 s) complexes but much smaller for Gd^{3+} complexes (2.4 ms), due to enhanced $T_1 \rightsquigarrow S_0$ nonradiative relaxation of the triplet state in the presence of Gd^{3+}.

In addition to ISC, the ET efficiency from the triplet to Ln^{3+} is critical in obtaining a high luminescent quantum yield.[33] The location of the triplet energy level is crucial in the sensitization of the lanthanide, for which the energy gap is said to range between 2500 and 5000 cm^{-1} above the luminescent state of the Ln^{3+}.[20,34] The downhill energy cascade then follows to promote the forward ET rate from the triplet state to Ln^{3+} and at the same time prevent the back ET. A significant correlation has been identified between the luminescence quantum yield and the ET rates.[27,35] Despite challenges in discerning the ET rate from the triplet state to the Ln^{3+}, employing Eu^{3+} complexes as a demonstration, it has been estimated using theory and experiment.[19,36]

To elucidate the excited dynamics in lanthanide complexes, which occur within the ultrafast time scale of picoseconds to nanoseconds, a spectroscopic technique capable of investigating this range is necessary. Femtosecond transient absorption spectroscopy (fs-TAS) can be employed to investigate the excited state properties of organic lanthanide complexes.[37−39] Mara et al. demonstrated that the depopulation of the triplet state to the $^5D_1$ state of Eu^{3+} occurs in the sub-picosecond scale, while that of the Gd-analog falls within the nanosecond range.[26] Through an analysis of NIR-emitting Ln^{3+} complexes, Chong et al. concluded that the kinetic profiles obtained using fs-TAS can be essentially quantitative, correlating with the luminescence quantum yield.[40] Instead of fs-TAS, nanosecond-TAS (ns-TAS) was utilized to examine the depopulation rate of the triplet state in analogous Gd^{3+} and Yb^{3+} complexes, which exhibited slower depopulation rates compared to the luminescent Er^{3+} analog.[41] By calculating the difference between the ground state and excited state absorption at a certain wavelength of the complex at different time delays, the change in optical density, $\Delta OD(\lambda, t)$ can be obtained from fs-TAS, which can be defined as

$$\Delta OD(\lambda, t) = -\Delta \log T(\lambda, t) = -\log\left(\frac{T(\lambda, t)}{T_0(\lambda, t)}\right) = -\log\frac{I_{pump}}{I_{unpump}} \quad (1)$$

where $T(\lambda, t)$ and $T_0(\lambda, t)$ are respectively the transmittance with pump light (exciting ray) and without pump light; I_{pump} and I_{unpump} are the transmitted light intensity of the probe (detection ray) with pump and without pump, respectively.

https://doi.org/10.1021/jacsau.4c00468
JACS Au 2024, 4, 3813−3822

Often, the rise time of the lanthanide luminescence is scrutinized to monitor the dynamics of the triplet state. However, the rise lifetime of the luminescent state may be unrelated to the triplet decay lifetime.[42] This could indicate that the ET from the antenna to the metal ion does not occur directly to the luminescent Ln^{3+} state. Furthermore, a previous study concerning the Sm^{3+} complex suggested that the receiving state of Sm^{3+} is slightly higher than the luminescent state.[43] The transfer from the triplet state to the relevant energy state of a lanthanide ion can be studied by employing fs-TAS at the picosecond scale. Therefore, we hypothesized that ET occurs from the triplet state to the nearest energy state of the Ln^{3+} (as shown in Figure 1a) if there are intermediate states, rather than directly to the luminescent state of the Ln^{3+}, as conventionally posited. To demonstrate the validity of our hypothesis, it is crucial to investigate the impact of different Ln^{3+} ions on (i) the ISC rate, by observing the triplet rise lifetime; and (ii) the ET rate to the relevant Ln^{3+} ion, by observing the T_1 decay rate, with the aid of fs-TAS. In this work, we utilize spectroscopic studies on five different systems, **Ln(TTA)$_3$·2H$_2$O**, **Lnphen(TTA)$_3$**, **LnL^a**, **LnL^b**, and **LnL^c** (Figure 1b) to resolve these questions and investigate the photophysical processes more deeply. These systems can be separated into three different categories, which are β-diketone-based, cyclen-based, and peptide-based ligands, to demonstrate the universality of the proposed mechanism. We opted to include β-diketone-based complexes in our study because they have been extensively investigated for mechanistic studies.[27,44,45] In addition, we chose cyclen-based and peptide-based complexes,[6,46−48] as they are commonly used in biological applications due to their effectiveness in biological systems.

RESULTS AND DISCUSSION

Lanthanide complexes typically luminesce in both the visible and near-infrared (NIR) regions, depending upon the particular metal ion. Inspecting the luminescent properties for the **Ln(TTA)$_3$·2H$_2$O** series, we find that visible emission is observed for Ln = Sm, Eu, and Tb (Figure S12), whereas NIR emission is observed for Nd, Sm, Yb, and Er (Figure S13). Ligand singlet emission is observed for Ln = Lu, Gd, and Tb at room temperature (RT) (Figure S12).

As previously highlighted, the fs-TAS can be employed to explore the dynamics of excited states that occur within the picosecond time scale. The RT fs-TAS of the three sets of complexes across the Ln^{3+} series show a similar profile shape for the same complexes (Figures 3, S18−S24, S50−S54, S56−S58, S60, S61, S63, S64) since they are essentially ligand-based. As demonstrated using **Ln(TTA)$_3$·2H$_2$O**, Ln = Sm, Eu, the spectral shape remains invariant despite the solvent environment (Figures S39−S42, S45−S47).

The analysis of TAS spectra indicates that a positive change in optical density (+ΔOD) can be attributed to an excited state absorption, while a negative change in optical density (−ΔOD) can correspond to emissions from the sample. As seen in Figure 2, we can classify the spectra into three different regions for **Ln(TTA)$_3$·2H$_2$O**: (i) **R^I**, with +ΔOD at ca. 390 nm; (ii) **R^{II}**, with −ΔOD at 425−500 nm; and (iii) **R^{III}**, with maximum +ΔOD at ca. 600 nm. We associate region **R^I** with the ligand's singlet−singlet absorption band from the first singlet state, $S_1 \rightarrow S_n$; **R^{II}** to the stimulated (and spontaneous) emission from the ligand; and **R^{III}** to triplet−triplet ($T_1 \rightarrow T_n$) absorption (Figure 2). The assignments of these bands are

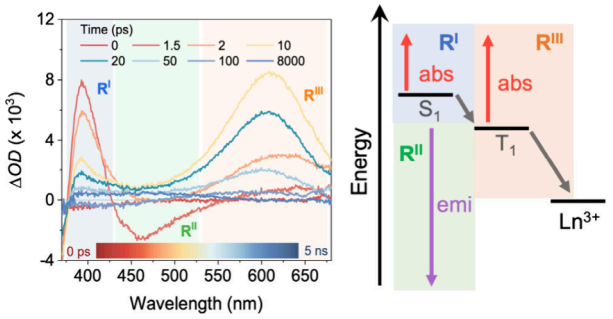

Figure 2. Selected transient absorption spectra at specific time scales for **Sm(TTA)$_3$·2H$_2$O**. The spectra are separated into the three regions: **R^I** with +ΔOD (singlet−singlet absorption), **R^{II}** with −ΔOD (spontaneous and stimulated emission), and **R^{III}** with +ΔOD (triplet−triplet absorption). The positive or negative ΔOD in the TAS spectra can correspond to different transitions, as illustrated in the Jablonski diagram. λ_{exc} = 355 nm.

supported by the similar fs-TAS shape of Eu(DBM)$_3$·H$_2$O.[49] Region **R^{II}** is overlapped by **R^I** and **R^{III}**, and this distorts its time profile. The effective lifetime of stimulated emission depends upon the radiation density and differs from that of spontaneous emission. A minor red-shift in the region **R^{III}** and a minor blue-shift in the region **R^I** are observed for all complexes. This indicates the possibility of (i) a shift in the energy gap due to vibronic or relaxation processes or (ii) another excited state being involved.

It is worth noting that despite different systems, the depopulation rate of the **R^{III}** region is always faster in the case of Sm^{3+}, compared to that of Eu^{3+}, as demonstrated in Figure 3. Monitoring at the **R^{III}** region (peak at ca. 600 nm) in Figure 3, the ΔOD goes back to zero at least 1 order of magnitude faster in the case of Sm^{3+} compared with that for Eu^{3+}. This is unexpected since the luminescent energy states of Sm^{3+} ($^4G_{5/2}$) and of Eu^{3+} ($^5D_0$) are at similar energies, located at 17 742 and 17 208 cm^{-1}, respectively. This indicates that the ET does not occur directly to the luminescent state of the Ln^{3+}, as discussed in the latter part of this manuscript.

The **R^{III}** kinetics profiles for the **Ln(TTA)$_3$·2H$_2$O** series of complexes are shown in Figures 4a, S29 and Table 1. The triplet rise lifetimes, representing ISC, are short and similar (between 0.4 and 2.5 ps) except for much longer rise lifetimes for Ln = Gd and Lu. Similar results are also observed for the **Lnphen(TTA)$_3$** series (Table S3, Figures S48, S49). Interestingly, the introduction of the −phen moiety into the complex does not have a substantial impact on the behavior of the excited state dynamics at the ultrafast time scale. The singlet state in these cases has a smaller proportion of triplet character mixed into it. Monitoring the wavelength at region **R^I**, on the other hand, shows a similar fast population within ∼0.2 ps after excitation (Figure 4b). The decay lifetime at region **R^I** is about 0.1−1 ps, similar to the triplet rise time at **R^{III}**. There appears to be a longer lifetime component also, accompanied by a shift of the maximum by about 4 nm to shorter wavelength. We have simulated this behavior by the involvement of higher energy singlet states (denoted by S_n) (SI, Figure S71). Our excited state time-dependent density functional theory (TD-DFT) calculation demonstrates that there are six lower lying triplet states below S_1 and three higher singlet states close in energy for **Lu(TTA)$_3$·2H$_2$O**. The orbital transitions for the excited singlet state demonstrate inter-TTA ET, while a transition within the same TTA moiety is observed

https://doi.org/10.1021/jacsau.4c00468
JACS Au 2024, 4, 3813−3822

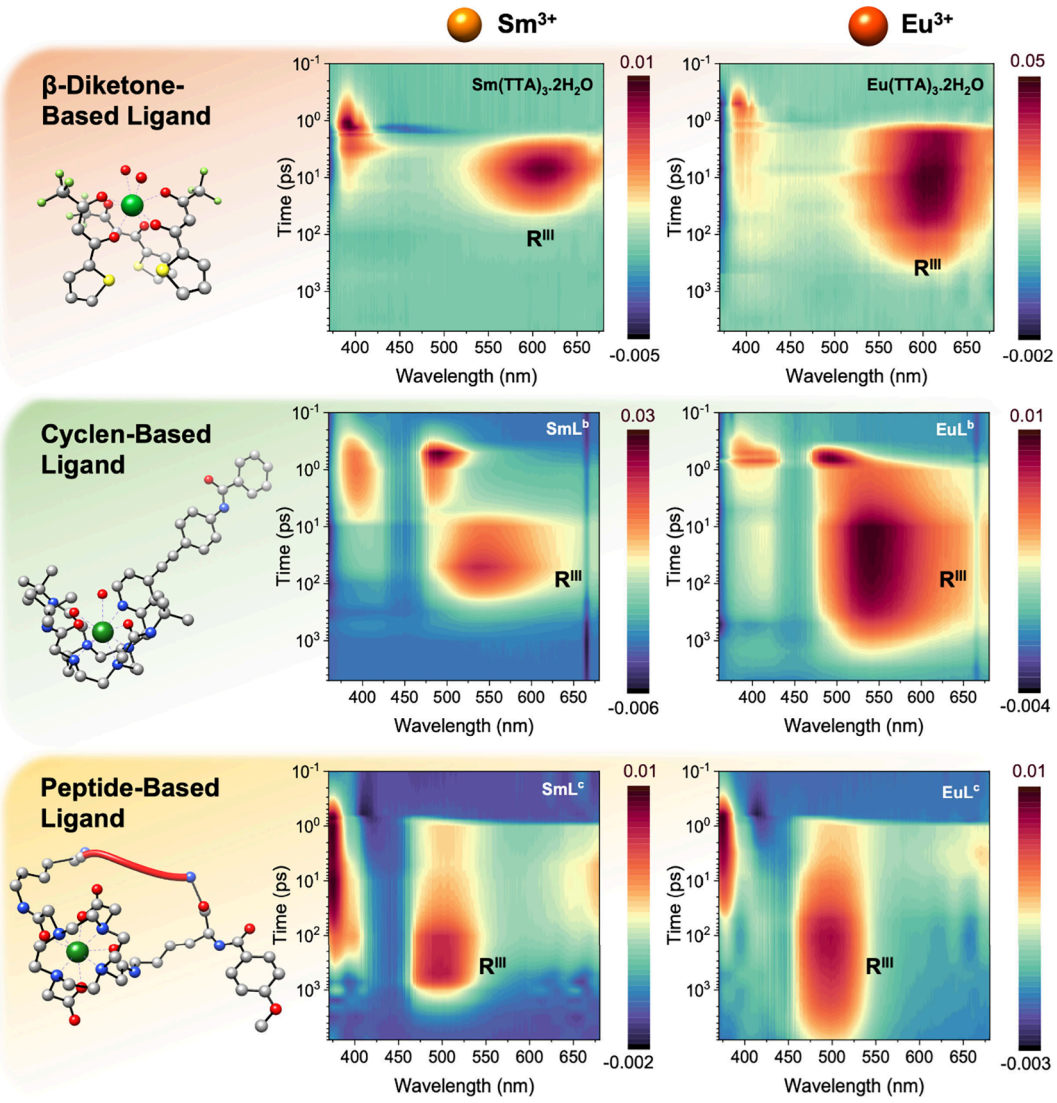

Figure 3. 3D plot of the fs-TAS of 100 μM **Ln(TTA)$_3$·2H$_2$O**, **LnL^b**, and **LnL^c** in $CHCl_3$ from 0.1 ps to 5 ns, separated in different categories. The time delay is plotted against wavelength, while the ΔOD is plotted as a color bar from positive change (red) to negative change (blue) as indicated. Across all categories, the +ΔOD at $\mathbf{R^{III}}$ (as labeled) undergoes a quicker return to zero in Sm^{3+} as compared to Eu^{3+}, despite the similar energy of the luminescent state of Eu^{3+} and Sm^{3+}. This indicates that the transfer from the triplet state is to the higher lying energy states of the Ln^{3+}.

for the triplet states (Figures 4c, S68). The possibilities of ET from the higher energy singlet states to the triplet states cannot be ruled out. Despite the presence of a correlation between the decay of $\mathbf{R^I}$ and the rise of $\mathbf{R^{III}}$, no clear relationship has been found between the depopulation rate of $\mathbf{R^{II}}$ (ca. 1 ps across the series, Table 1) and the depopulation of either the singlet or triplet state. This indicates that the ligand emission lifetime comprises contributions not only from spontaneous emission but also from stimulated emission. It is worth noting that while similar fs-TAS spectral shapes can be observed for different solvents as discussed earlier, there is a significant variation in the kinetics, depending on the solvent polarity (Table S2). The triplet depopulation rate is observed to be longest in chloroform and fastest in methanol, which highlights the influence of the solvent on the excited state dynamics, which is not uncommon for lanthanide complexes.[50]

The deconvolution of the TAS spectra can be represented by the evolution associated spectra (EAS) and the species associated spectra (SAS). With the aid of global fitting employing the spectrotemporal model,[51] the sequential EAS represent the evolution of the spectra, with the rise and decay rate constants.

The population of the species that are associated with the spectral evolution can then be plotted in the SAS. The TAS spectra recorded are well fitted with three (Figures S30−S36) rather than two components (Figures S37, S38). It is not appropriate to fit the data with two components because then both species would not be simultaneously populated at time zero (Figures S37, S38). Considering the fitting with three components, we suggest that the first EAS component is associated with the population of the singlet states, exhibiting a fast decay time constant. The second component, comprising a mixture of regions $\mathbf{R^I}$ and $\mathbf{R^{III}}$, arises from the combination of processes from the slower decay of neighboring singlet states and nonradiative cascade through triplet states above T_1 (Figure 4c, Table S4). A shift in the maximum ΔOD is evident in both regions. The third component, with time constants between 13 and 300 ps for different luminescent lanthanide ions (and unlimited ∼22 ns for Ln = Gd, where

https://doi.org/10.1021/jacsau.4c00468
JACS Au 2024, 4, 3813−3822

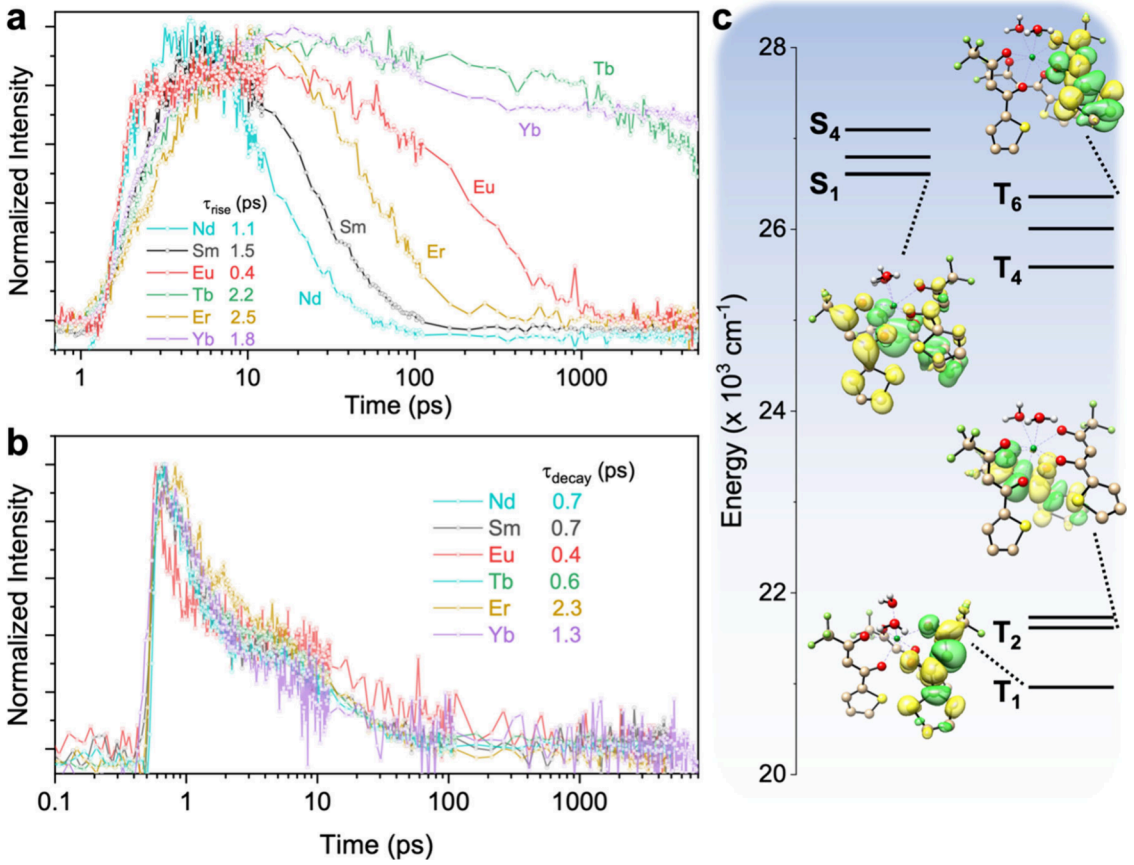

Figure 4. Kinetics monitored at region (a) $\mathbf{R^{III}}$ and (b) $\mathbf{R^{I}}$ on a logarithmic time scale, corresponding to (a) the population of the triplet state and (b) depopulation of the singlet state of 100 μM $\mathbf{Ln(TTA)_3{\cdot}2H_2O}$ in $CHCl_3$, across the Ln series. The rise lifetime of region $\mathbf{R^{III}}$ and the decay lifetime of region $\mathbf{R^{I}}$ for different lanthanides are included in the figures. λ_{exc} = 355 nm. (c) The calculated energy levels and selected orbital transitions of $\mathbf{Lu(TTA)_3{\cdot}2H_2O}$. Green: decrease in electron density; yellow: increase in electron density. Isovalue: 0.001.

Table 1. Rise and Decay Lifetimes of 100 μM $\mathbf{Ln(TTA)_3{\cdot}2H_2O}$ in $CHCl_3$ Monitored at Regions $\mathbf{R^{I}}$ and $\mathbf{R^{III}}$ of the fs-TAS, λ_{exc} = 355 nm

	R^I	R^{III}	
Ln	τ_{decay} (ps)	τ_{rise} (ps)	τ_{decay} (ps)
Nd	0.7	1.1	13.3
Sm	0.7	1.5	24.8
Eu	0.4	0.5	300
Gd	1.3	5.9	22 000[a]
Tb	0.6	2.2	102
			16 700
Er	2.3	2.5	53.1
Yb	1.3	1.8	6320
Lu	0.6	53.4	–[a]

[a]The long $\mathbf{R^{III}}$ decay lifetime of $\mathbf{Gd(TTA)_3{\cdot}2H_2O}$ is due to the absence of a receiving state, while that for $\mathbf{Lu(TTA)_3{\cdot}2H_2O}$ is outside the detection range.

there is no receiving lanthanide state, Table 1), corresponds to the triplet decay from T_1.

The shortest rise lifetime for population of the triplet state for $\mathbf{Ln(TTA)_3{\cdot}2H_2O}$ occurs for Ln = Eu (Figure 4a). A similar observation can be seen from a recent fs-TAS study of $NaYF_4$@$NaGdF_4$ nanoparticles with a surface coating of a carbazole derivative,[52] where the shortest rise lifetime (9.3 ps) also occurs for Eu^{3+}. The ISC rate is sensitive to the admixture of singlet and triplet states, which depends upon the nature of the perturbing state and its energy separation from S_1 and T_1. The fast ISC rate also agrees with the calculated rate, found to be in the picosecond range, which has been associated with the involvement of the Eu^{3+} $^7F_1$ state.[19,36] Hence, the involvement of f-electrons is likely to influence the ISC rate. A model that takes into account the influence of f-electrons across the Ln^{3+} series is currently being developed for a systematic explanation of the observed results.

The prevailing research studies on Eu^{3+} complexes suggest that the ET from an antenna takes place to the $^5D_1$ energy level.[26,36,53] Our previous calculations on the system $\mathbf{Eu(TTA)_3{\cdot}2H_2O}$ showed that the pathway for singlet ET is feasible, but we were unable to calculate the triplet ET rate due to the exchange mechanism.[44] The ET rates from the triplet state by multipolar mechanisms were found to be of minor importance, so that if ET does occur from the triplet state, it must be by the exchange mechanism. It turns out that we underestimated the ISC and triplet decay rates in our simulations by several orders of magnitude. Herein, we observe the experimental triplet decay lifetime of 0.27 ± 0.03 ns for Eu^{3+}, in both polar and nonpolar solvents (Figures 4a, S43, S44). We therefore present revised kinetic simulations of the antenna-metal ET process which occurs through the triplet state. The revised kinetics for the triplet and $^5D_1$ states are displayed in Figure 5a, and the other graphs are included in the Supporting Information.

As demonstrated in Figure 3, the depopulation rate of the triplet state is always faster for Sm^{3+} compared to Eu^{3+}.

https://doi.org/10.1021/jacsau.4c00468
JACS Au 2024, 4, 3813−3822

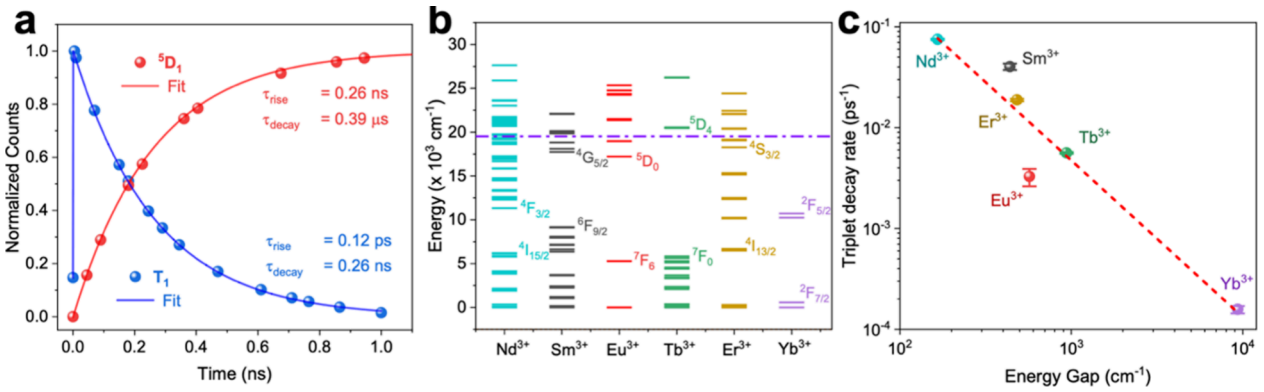

Figure 5. (a) Calculated rise and decay curves for T_1 and $^5D_1$ states of **Eu(TTA)$_3$·2H$_2$O** using the rate equation parameters in Table S5. (b) The relevant energy levels of Ln^{3+} with labeled selected states. The triplet state of **Ln(TTA)$_3$·2H$_2$O** is labeled as a purple dash-dotted line located at 19886 cm^{-1}. (c) The RT decay rate of the triplet state plotted against the absolute energy difference between the triplet state and the nearest level of the respective Ln^{3+} in logarithmic scale.

Considering Ln^{3+} across the series in the same complex system, as shown in Figure 4a, the depopulation rate of the triplet state of **Ln(TTA)$_3$·2H$_2$O** follows the trend of Nd > Sm > Er > Eu > Yb, Tb. Hence, the depopulation rate at RT can be rationalized by the difference in the energy gap between the first triplet state and the nearest Ln^{3+} receiving state. As demonstrated in Figure 5b, the near resonance between the donor (purple line, triplet energy level located at 19 886 cm^{-1})[44] and acceptor energy levels is expected to lead to rapid ET in the cases of Nd^{3+}, Sm^{3+}, or Er^{3+}. Figure 5c shows a slower decay rate for Ln^{3+} with receiving states that are more distant from the triplet state energy. Similar plots are observed for the **Lnphen(TTA)$_3$** complexes, where the depopulation rate follows Nd > Sm > Eu > Yb (Figures S55). This graph is similar to that for the well-known energy gap law of Riseberg et al.:[54,55]

$$W = C\exp(\alpha\Delta E) \tag{2}$$

where W is the nonradiative rate; C and α are constants; and ΔE is the energy gap between levels. However, that scenario refers to the intraconfigurational multiphonon relaxation as determined by phonons of maximum energy. The present case, Figure 5c, refers to organometallic systems with much higher vibrational frequencies and much smaller energy gaps. The T_1 → Ln^{3+} rate is faster when the gap to the nearest receiving state is smaller.

It is significant to highlight that since the depopulation rate of the triplet is heavily influenced here, the energy gap plays an important role in determining this ET step. As mentioned before, the participation of f-electrons is one of the reasons causing the fastest ISC observed for Eu complexes, which, to some extent, suggests that the possibility of overlapping spin populations between the lanthanide ion and organic chromophore cannot be ruled out.[56]

In light of Eu complexes, Faustino et al.[57] measured the kinetics of $^5D_1$ population and decay at RT for solid-state **Eu(TTA)$_3$·2H$_2$O**. The time to maximum emission intensity (t_{max}) was 84 ns, and the $^5D_1$ decay lifetime (τ_A) was 0.4 μs. To calculate the triplet decay lifetime, the formula comprising a donor (D) and acceptor (A) can be written as

$$t_{max} = \frac{1}{(\tau_D^{-1} - \tau_A^{-1})}\ln\left[\frac{\tau_A}{\tau_D}\right] \tag{3}$$

where the triplet decay lifetime, τ_D, is calculated to be 30 ns. This is 2 orders of magnitude slower than in our present solution study and presumably indicates a much greater nonradiative contribution in solution. Our measurement for the triplet decay lifetime is not unusual, with the value 0.32 ns recorded for $[Eu(DPA)_3]^{3-}$ in solution[58] and 0.88 ns for Eu^{3+} in solid-state nanoparticles.[52] The rise lifetime of the subsequent luminescent state, $^5D_0$, is in the sub-millisecond regime.[42] The major point here is that the rise lifetime of the luminescent state is unrelated to the triplet decay lifetime if there are intermediate states. This is the case in literature reports of microsecond rise lifetimes for luminescent states of Nd^{3+},[59,60] Sm^{3+},[61] Er^{3+},[62] and Yb^{3+}.[59] Consequently, ET occurs from the triplet state to the nearest energy state of the Ln^{3+}, as shown in Figure 1a, in situations where intermediates are present, instead of directly to the luminescence state of the Ln^{3+} as commonly suggested. It is also worth emphasizing that the depopulation of the triplet state outpaces the quenching rate (~10^7 s^{-1} time scale) by oxygen in solution;[63,64] hence the emission intensity of Eu^{3+} remains largely unaffected by the oxygen content.

CONCLUSIONS

Through the use of ultrafast TAS, TD-DFT calculations, and a rate equation model, we have gained a deeper insight into the ET, where the ET occurs from the triplet state to the intermediate states, if they exist, rather than directly to the luminescence state of the Ln^{3+}. An energy gap dependence has been found for the triplet decay rate by matching the energy gap with the nearest receiving state of the Ln^{3+}. The diverse structures used in this work support the universality of this proposition. However, it is significant to underscore that ISC plays a pivotal role in determining the luminescence of the Ln^{3+}. The ISC rate is fastest for Eu^{3+}, and a deeper understanding of the role of 4f electrons is required to explain this. Nevertheless, our discovery sheds light on the ET from the triplet state to the Ln^{3+}. The tuning of the energy level of the triplet state should correspond with the nearest receiving state, rather than the luminescence state of the trivalent lanthanide ions, so as to optimize the light harvesting from the antenna to enhance the luminescence of the complex for use in diverse applications.

https://doi.org/10.1021/jacsau.4c00468
JACS Au 2024, 4, 3813−3822

METHODS

Syntheses

Ln(TTA)$_3$·2H$_2$O. 2-Thenoyltrifluoroacetone (TTA, 3 equiv., 3 mmol, 0.666 g) was first dissolved in 10 mL of EtOH, and 3 mL of 1.0 M NaOH solution was added to adjust the pH of the solution. The solution was heated to 60 °C, and an aqueous solution of $LnCl_3$ (Ln = Nd, Sm, Eu, Gd, Tb, Er, Yb, Lu, 1 equiv., 1 mmol) was added dropwise. The solution was allowed to react for 2 h, and the contents were dried in a rotary evaporator. The solid was filtered and washed with hexane and cold water and dried in a desiccator.

Lnphen(TTA)$_3$. The **Lnphen(TTA)$_3$** samples were synthesized by the literature method.[65] Typically, TTA (3 mmol) and 1,10-phenanthroline (phen) (1 mmol) were dissolved in 15 mL of ethanol in a flask, with stirring at room temperature. Then, the pH of the solution was adjusted to 7.0 by the addition of NaOH solution (1.0 M). After that, 1 mmol of $LnCl_3$ solution in 5.0 mL of deionized water was added into the above mixture at 60 °C with vigorous stirring for 1.0 h to ensure a complete precipitation. The precipitate was finally filtered, washed repeatedly with ethanol and water, and dried overnight under vacuum. The yields and characterizations are included in a previous publication.[66]

LnL^a. The synthetic route is outlined in Figure S1. Briefly, the azide-containing antenna (**S7**) was constructed via multistep reactions, which include two Sonogashira couplings and direct amination of the methyl ester with an azide-containing linker (**S6**). The antenna was then installed onto the cyclen core (^{t}Bu-DO3A, **S8**), and the corresponding lanthanide complexes (**Ln-N$_3$**) were obtained after deprotection of the *tert*-butyl ester and coordination with the lanthanide ion. The yields and characterizations are included in a previous publication.[6]

LnL^b. The synthetic route is outlined in Figure S2. The **S3** was obtained by the same procedure as shown in Figure S1. The **S3** was further converted to **S11** by conducting Sonogashira coupling with **S10**. The antenna **S11** was then installed onto the cyclen core (tris-^{t}Bu-DO3AM, **S12**) to give **S13**, and the corresponding lanthanide complexes (**LnL^b**) were obtained after coordination with the lanthanide ion. The yield and characterization is included in a previous publication.[67]

LnL^c. The synthetic route is outlined in Figure S3. Briefly, the solid-phase peptide synthesis (SPPS) was conducted on Rink AM resin to give a N-capped Lys(Mtt)-Arg(Pbf)-Gly-Asp(^{t}Bu)-Lys(Mtt) (**S14**). The Mtt protecting groups on two Lys side chains were removed to release two free amine groups, and bromoacetic acid was further installed to give **S16**. The bis-Alloc-protected cyclen building block **S17** was then incorporated onto the peptide to give **S18**. And the two Alloc protecting groups were removed to release two amine groups for installing antenna **S19**. The global cleavage and deprotecting were conducted to give desired cyclen-embedded cyclic pepetide **S21**, and the corresponding lanthanide complexes (**LnL^c**) were obtained after coordination with the lanthanide ion. The yield and characterization are included in a previous publication.[46]

Nuclear Magnetic Resonance Spectroscopy

The NMR spectra reported were obtained from a Bruker UltraShield 400 Plus NMR spectrometer. The ^{1}H chemical shifts were referenced to corresponding solvent peaks of MeOD-d_4 at 3.31 ppm. The ^{13}C chemical shifts were referenced to corresponding solvent peaks of MeOD-d_4 at 49.00 ppm.

Steady State Photophysical Characterization

FT-IR spectra were recorded by a PerkinElmer FT-IR Spectrum Two instrument. The ultraviolet−visible absorption spectra were measured in solution in the range 200−800 nm by a PerkinElmer LAMBDA 1050+ UV/vis/NIR double beam spectrophotometer. The emission, excitation spectra, and luminescence decay curves were recorded using a Horiba Fluorolog-3 instrument with a 450 W xenon lamp. The signal was detected by a Hamamatsu R928 photomultiplier and corrected with excitation and emission correction factors to eliminate response characteristics. A custom-made liquid nitrogen cryostat with an NMR tube sample holder was employed for 77 K studies. A 10 mm path length cuvette was used for all room-temperature measurements except where specified.

Femtosecond Transient Absorption

Room-temperature femtosecond transient absorption measurements were performed using an amplified laser system (Spitfire ACE, Spectra Physics) as the excitation source, delivering ca. 100 fs 800 nm laser pulses at a 1 kHz repetition rate. The Maitai laser system is centered with a wavelength of 800 nm and 6 mJ/pulse energy with a pulse time width of 85 fs. For the beam, approximately 0.1 mJ of the output from the laser excitation source was focused onto a 3 mm CaF_2 window to generate a white light continuum probe pulse in the visible region from ca. 350 to 650 nm. For the pump, the remainder of the laser output is used to pump into the Optical Parametric Amplifier (OPA) to tune to the desired excitation wavelength of the sample, with a pump fluence of roughly 2 mJ/cm^2 (~20 μJ). The absorption is collected using an MS260i automated spectrograph. In the spectrometer, we used a 1000 ms integration time and an average of 3 spectra at each delay position. The samples were stirred using a magnetic stir bar throughout the measurement. The resulting time traces were analyzed globally using GloTarAn[68] and the R package TIMP.[69] A 2 mm path length cuvette was used for measurements.

Computational Modeling

The optimization of all structures by DFT calculations, both in gas and in solvent conditions, was performed using the Gaussian16 package.[70] The nature of each stationary point was characterized using frequency calculations. Molecules were built using Avogadro software.[71] Excited state calculations were performed using the ORCA 4.2 suite of programs.[72,73] The integration grid was set to Lebedev 590 points with the final grid of Lebedev 770 points. Geometry optimizations and free-energy calculations were performed at the PBE0-D3/def2-TZVP level of theory, with the Stuttgart in-core large core relative effective core potentials (LCRECP)[74,75] and basis sets for the lanthanide ions. TD-DFT calculations were performed with the same level of theory using the Pople solver. However, a small core relative effective core potential (MWB28)[76] was employed for TD-DFT calculations to take into account the participation of f-electrons. Spin−orbit coupling was considered. The simulated absorption spectra employed the bandwidth of 3000 cm^{-1}. UCSF Chimera (version 1.14)[77] was used for the visualization of geometries and orbitals. Maple 2021 was employed for computations involving the rate equation model.

ASSOCIATED CONTENT

Supporting Information

The Supporting Information is available free of charge at https://pubs.acs.org/doi/10.1021/jacsau.4c00468.

Synthesis and methodologies, structural and photophysical characterizations for complexes, cryogenic photoluminescence spectra and lifetime analysis, additional TAS data with kinetics analysis, additional TD-DFT calculation data and kinetics model for the ET process (PDF)

AUTHOR INFORMATION

Corresponding Authors

Loïc J. Charbonnière − *Equipe de Synthèse Pour l'Analyse (SynPA), Institut Pluridisciplinaire Hubert Curien (IPHC), UMR 7178, CNRS, Université de Strasbourg, ECPM, 67087 Strasbourg Cedex, France;* orcid.org/0000-0003-0328-9842; Email: l.charbonn@unistra.fr

Peter A. Tanner − *Department of Applied Biology and Chemical Technology, The Hong Kong Polytechnic University, Kowloon, Hong Kong S.A.R. 999077, People's*

https://doi.org/10.1021/jacsau.4c00468
JACS Au 2024, 4, 3813−3822

Republic of China; orcid.org/0000-0002-4681-6203; Email: peter.a.tanner@gmail.com

Ka-Leung Wong − *Department of Applied Biology and Chemical Technology, The Hong Kong Polytechnic University, Kowloon, Hong Kong S.A.R. 999077, People's Republic of China;* orcid.org/0000-0002-3750-5980; Email: klgwong@polyu.edu.hk

Authors

Waygen Thor − *Department of Applied Biology and Chemical Technology, The Hong Kong Polytechnic University, Kowloon, Hong Kong S.A.R. 999077, People's Republic of China; Equipe de Synthèse Pour l'Analyse (SynPA), Institut Pluridisciplinaire Hubert Curien (IPHC), UMR 7178, CNRS, Université de Strasbourg, ECPM, 67087 Strasbourg Cedex, France; Department of Chemistry, Hong Kong Baptist University, Kowloon Tong, Hong Kong S.A.R. 999077, People's Republic of China;* orcid.org/0000-0002-4366-9113

Hei-Yui Kai − *Department of Applied Biology and Chemical Technology, The Hong Kong Polytechnic University, Kowloon, Hong Kong S.A.R. 999077, People's Republic of China;* orcid.org/0000-0001-9960-7467

Yik-Hoi Yeung − *Department of Applied Biology and Chemical Technology, The Hong Kong Polytechnic University, Kowloon, Hong Kong S.A.R. 999077, People's Republic of China*

Yue Wu − *Department of Chemistry, Hong Kong Baptist University, Kowloon Tong, Hong Kong S.A.R. 999077, People's Republic of China*

Tsz-Lam Cheung − *Department of Chemistry, Hong Kong Baptist University, Kowloon Tong, Hong Kong S.A.R. 999077, People's Republic of China;* orcid.org/0000-0002-4303-1494

Leo K. B. Tam − *Department of Applied Biology and Chemical Technology, The Hong Kong Polytechnic University, Kowloon, Hong Kong S.A.R. 999077, People's Republic of China;* orcid.org/0000-0002-2436-0057

Yonghong Zhang − *Department of Chemistry, Hong Kong Baptist University, Kowloon Tong, Hong Kong S.A.R. 999077, People's Republic of China; State Key Laboratory of Chemistry and Utilization of Carbon-Based Energy Resources, Key Laboratory of Oil and Gas Fine Chemicals, Ministry of Education & Xinjiang Uygur Autonomous Region, Urumqi Key Laboratory of Green Catalysis and Synthesis Technology, College of Chemistry, Xinjiang University, Urumqi 830046 Xinjiang, People's Republic of China;* orcid.org/0000-0002-7740-9408

Complete contact information is available at: https://pubs.acs.org/10.1021/jacsau.4c00468

Author Contributions

The manuscript was written through contributions of all authors. All authors have given approval to the final version of the manuscript. CRediT: **Waygen Thor** conceptualization, data curation, formal analysis, writing-original draft, writing-review & editing; **Hei-Yui Kai** data curation, formal analysis; **Yik-Hoi Yeung** data curation; **Yue Wu** data curation; **Tsz-Lam Cheung** data curation; **Leo K. B. Tam** data curation; **Yonghong Zhang** data curation; **Loïc J. Charbonnière** supervision, writing-review & editing; **Peter A. Tanner** formal analysis, supervision, writing-original draft, writing-review & editing; **Ka-Leung Wong** conceptualization, funding acquisition, supervision, writing-review & editing.

Notes

The authors declare no competing financial interest.

■ ACKNOWLEDGMENTS

K.-L.W. acknowledges financial assistance from the Hong Kong Research Grants Council No. 12300021, NSFC/RGC Joint Research Scheme (N_PolyU209/21), and the Centre for Medical Engineering of Molecular and Biological Probes (AoE/M 401/20).

■ ABBREVIATIONS

fs-TAS: femtosecond transient absorption spectroscopy; ET: energy transfer; NIR: near-infrared; EAS: evolution associated spectra; SAS: species associated spectra; ISC: intersystem crossing; RT: room temperature

■ REFERENCES

(1) Weissman, S. I. Intramolecular Energy Transfer The Fluorescence of Complexes of Europium. *J. Chem. Phys.* **1942**, *10* (4), 214−217.

(2) Moore, E. G.; Samuel, A. P. S.; Raymond, K. N. From Antenna to Assay: Lessons Learned in Lanthanide Luminescence. *Acc. Chem. Res.* **2009**, *42* (4), 542−552.

(3) Bünzli, J.-C. G. Lanthanide Luminescence for Biomedical Analyses and Imaging. *Chem. Rev.* **2010**, *110* (5), 2729−2755.

(4) Yang, Y.; Wang, P.; Lu, L.; Fan, Y.; Sun, C.; Fan, L.; Xu, C.; El-Toni, A. M.; Alhoshan, M.; Zhang, F. Small-Molecule Lanthanide Complexes Probe for Second Near-Infrared Window Bioimaging. *Anal. Chem.* **2018**, *90* (13), 7946−7952.

(5) Amoroso, A. J.; Pope, S. J. A. Using Lanthanide Ions in Molecular Bioimaging. *Chem. Soc. Rev.* **2015**, *44* (14), 4723−4742.

(6) Chau, H.-F.; Wu, Y.; Fok, W.-Y.; Thor, W.; Cho, W. C.-S.; Ma, P. a.; Lin, J.; Mak, N.-K.; Bünzli, J.-C. G.; Jiang, L.; Long, N. J.; Lung, H. L.; Wong, K.-L. Lanthanide-Based Peptide-Directed Visible/Near-Infrared Imaging and Inhibition of LMP1. *JACS Au* **2021**, *1* (7), 1034−1043.

(7) Knighton, R. C.; Soro, L. K.; Thor, W.; Strub, J.-M.; Cianférani, S.; Mély, Y.; Lenertz, M.; Wong, K.-L.; Platas-Iglesias, C.; Przybilla, F.; Charbonnière, L. J. Upconversion in a *d*−*f* [$RuYb_3$] Supramolecular Assembly. *J. Am. Chem. Soc.* **2022**, *144* (29), 13356−13365.

(8) Sun, G.; Ren, Y.; Song, Y.; Xie, Y.; Zhang, H.; Sun, L. Achieving Photon Upconversion in Mononuclear Lanthanide Molecular Complexes at Room Temperature. *J. Phys. Chem. Lett.* **2022**, *13* (36), 8509−8515.

(9) Charbonnière, L. J.; Nonat, A. M.; Knighton, R. C.; Godec, L. Upconverting Photons at the Molecular Scale with Lanthanide Complexes. *Chem. Sci.* **2024**, *15* (9), 3048−3059.

(10) Ghazy, A.; Lastusaari, M.; Karppinen, M. Excitation Wavelength Engineering through Organic Linker Choice in Luminescent Atomic/Molecular Layer Deposited Lanthanide−Organic Thin Films. *Chem. Mater.* **2023**, *35* (15), 5988−5995.

(11) Wang, X.; Wang, Y.; Wang, Y.; Liu, H.; Zhang, Y.; Liu, W.; Wang, X.; Wang, S. Color-Tunable X-Ray Scintillation Based on a Series of Isotypic Lanthanide−Organic Frameworks. *Chem. Commun.* **2020**, *56* (2), 233−236.

(12) Kido, J.; Okamoto, Y. Organo Lanthanide Metal Complexes for Electroluminescent Materials. *Chem. Rev.* **2002**, *102* (6), 2357−2368.

(13) Rubin, M. B.; Braslavsky, S. E. Quantum Yield: The Term and the Symbol. A Historical Search. *Photochem. Photobiol. Sci.* **2010**, *9* (5), 670−674.

(14) Wong, K.-L.; Bünzli, J.-C. G.; Tanner, P. A. Quantum Yield and Brightness. *J. Lumin.* **2020**, *224*, No. 117256.

(15) Malta, O. L.; Brito, H. F.; Menezes, J. F. S.; Silva, F. R. G. e.; Alves, S.; Farias, F. S.; de Andrade, A. V. M. Spectroscopic Properties

of a New Light-Converting Device Eu(thenoyltrifluoroacetonate)$_3$2-(dibenzylsulfoxide). A Theoretical Analysis Based on Structural Data Obtained from a Sparkle Model. *J. Lumin.* **1997**, *75* (3), 255−268.
(16) Beltrán-Leiva, M. J.; Cantero-López, P.; Zúñiga, C.; Bulhões-Figueira, A.; Páez-Hernández, D.; Arratia-Pérez, R. Theoretical Method for an Accurate Elucidation of Energy Transfer Pathways in Europium(III) Complexes with Dipyridophenazine (dppz) Ligand: One More Step in the Study of the Molecular Antenna Effect. *Inorg. Chem.* **2017**, *56* (15), 9200−9208.
(17) Zhang, Z.; He, L.; Feng, J.; Liu, X.; Zhou, L.; Zhang, H. Unveiling the Relationship between Energy Transfer and the Triplet Energy Level by Tuning Diarylethene within Europium(III) Complexes. *Inorg. Chem.* **2020**, *59* (1), 661−668.
(18) Malta, O. L. Mechanisms of Non-Radiative Energy Transfer Involving Lanthanide Ions Revisited. *J. Non-Cryst. Solids* **2008**, *354* (42), 4770−4776.
(19) Wu, L.; Fang, Y.; Zuo, W.; Wang, J.; Wang, J.; Wang, S.; Cui, Z.; Fang, W.; Sun, H.-L.; Li, Y.; Chen, X. Excited-State Dynamics of Crossing-Controlled Energy Transfer in Europium Complexes. *JACS Au* **2022**, *2* (4), 853−864.
(20) Latva, M.; Takalo, H.; Mukkala, V.-M.; Matachescu, C.; Rodríguez-Ubis, J. C.; Kankare, J. Correlation Between the Lowest Triplet State Energy Level of the Ligand and Lanthanide(III) Luminescence Quantum Yield. *J. Lumin.* **1997**, *75* (2), 149−169.
(21) Hasegawa, Y.; Kitagawa, Y. Luminescent Lanthanide Coordination Polymers with Transformative Energy Transfer Processes for Physical and Chemical Sensing Applications. *J. Photochem. Photobiol., C* **2022**, *51*, No. 100485.
(22) Yang, C.; Fu, L.-M.; Wang, Y.; Zhang, J.-P.; Wong, W.-T.; Ai, X.-C.; Qiao, Y.-F.; Zou, B.-S.; Gui, L.-L. A Highly Luminescent Europium Complex Showing Visible-Light-Sensitized Red Emission: Direct Observation of the Singlet Pathway. *Angew. Chem., Int. Ed.* **2004**, *43* (38), 5010−5013.
(23) D'Aléo, A.; Picot, A.; Beeby, A.; Gareth Williams, J. A.; Le Guennic, B.; Andraud, C.; Maury, O. Efficient Sensitization of Europium, Ytterbium, and Neodymium Functionalized Tris-Dipicolinate Lanthanide Complexes through Tunable Charge-Transfer Excited States. *Inorg. Chem.* **2008**, *47* (22), 10258−10268.
(24) Butler, S. J.; Delbianco, M.; Lamarque, L.; McMahon, B. K.; Neil, E. R.; Pal, R.; Parker, D.; Walton, J. W.; Zwier, J. M. EuroTracker® Dyes: Design, Synthesis, Structure and Photophysical Properties of Very Bright Europium Complexes and Their Use in Bioassays and Cellular Optical Imaging. *Dalton Trans.* **2015**, *44* (11), 4791−4803.
(25) D'Aléo, A.; Pointillart, F.; Ouahab, L.; Andraud, C.; Maury, O. Charge Transfer Excited States Sensitization of Lanthanide Emitting from the Visible to the Near-Infrared. *Coord. Chem. Rev.* **2012**, *256* (15), 1604−1620.
(26) Mara, M. W.; Tatum, D. S.; March, A.-M.; Doumy, G.; Moore, E. G.; Raymond, K. N. Energy Transfer from Antenna Ligand to Europium(III) Followed Using Ultrafast Optical and X-ray Spectroscopy. *J. Am. Chem. Soc.* **2019**, *141* (28), 11071−11081.
(27) Carneiro Neto, A. N.; Moura, R. T., Jr.; Carlos, L. D.; Malta, O. L.; Sanadar, M.; Melchior, A.; Kraka, E.; Ruggieri, S.; Bettinelli, M.; Piccinelli, F. Dynamics of the Energy Transfer Process in Eu(III) Complexes Containing Polydentate Ligands Based on Pyridine, Quinoline, and Isoquinoline as Chromophoric Antennae. *Inorg. Chem.* **2022**, *61* (41), 16333−16346.
(28) Baryshnikov, G.; Minaev, B.; Ågren, H. Theory and Calculation of the Phosphorescence Phenomenon. *Chem. Rev.* **2017**, *117* (9), 6500−6537.
(29) Arppe, R.; Kofod, N.; Junker, A. K. R.; Nielsen, L. G.; Dallerba, E.; Just Sørensen, T. Modulation of the Photophysical Properties of 1-Azathioxanthones by Eu^{3+}, Gd^{3+}, Tb^{3+}, and Yb^{3+} Ions in Methanol. *Eur. J. Inorg. Chem.* **2017**, *2017* (44), 5246−5253.
(30) Beltrán-Leiva, M. J.; Solis-Céspedes, E.; Páez-Hernández, D. The Role of the Excited State Dynamic of the Antenna Ligand in the Lanthanide Sensitization Mechanism. *Dalton Trans.* **2020**, *49* (22), 7444−7450.
(31) Isaac, M.; Denisov, S. A.; Roux, A.; Imbert, D.; Jonusauskas, G.; McClenaghan, N. D.; Sénèque, O. Lanthanide Luminescence Modulation by Cation−π Interaction in a Bioinspired Scaffold: Selective Detection of Copper(I). *Angew. Chem., Int. Ed.* **2015**, *54* (39), 11453−11456.
(32) Tobita, S.; Arakawa, M.; Tanaka, I. Electronic Relaxation Processes of Rare Earth Chelates of Benzoyltrifluoroacetone. *J. Phys. Chem.* **1984**, *88* (13), 2697−2702.
(33) Hasegawa, Y.; Kitagawa, Y.; Nakanishi, T. Effective Photosensitized, Electrosensitized, and Mechanosensitized Luminescence of Lanthanide Complexes. *NPG Asia Mater.* **2018**, *10* (4), 52−70.
(34) Steemers, F. J.; Verboom, W.; Reinhoudt, D. N.; van der Tol, E. B.; Verhoeven, J. W. New Sensitizer-Modified Calix[4]arenes Enabling Near-UV Excitation of Complexed Luminescent Lanthanide Ions. *J. Am. Chem. Soc.* **1995**, *117* (37), 9408−9414.
(35) Aquino, L. E. d. N.; Barbosa, G. A.; Ramos, J. d. L.; O. K. Giese, S.; Santana, F. S.; Hughes, D. L.; Nunes, G. G.; Fu, L.; Fang, M.; Poneti, G.; Carneiro Neto, A. N.; Moura, R. T., Jr.; Ferreira, R. A. S.; Carlos, L. D.; Macedo, A. G.; Soares, J. F. Seven-Coordinate Tb^{3+} Complexes with 90% Quantum Yields: High-Performance Examples of Combined Singlet- and Triplet-to-Tb^{3+} Energy-Transfer Pathways. *Inorg. Chem.* **2021**, *60* (2), 892−907.
(36) Zhang, Q.; Wu, L.; Cao, X.; Chen, X.; Fang, W.; Dolg, M. Energy Resonance Crossing Controls the Photoluminescence of Europium Antenna Probes. *Angew. Chem., Int. Ed.* **2017**, *56* (27), 7986−7990.
(37) Galán, L. A.; Reid, B. L.; Stagni, S.; Sobolev, A. N.; Skelton, B. W.; Cocchi, M.; Malicka, J. M.; Zysman-Colman, E.; Moore, E. G.; Ogden, M. I.; Massi, M. Visible and Near-Infrared Emission from Lanthanoid β-Triketonate Assemblies Incorporating Cesium Cations. *Inorg. Chem.* **2017**, *56* (15), 8975−8985.
(38) Han, S.; Yi, Z.; Zhang, J.; Gu, Q.; Liang, L.; Qin, X.; Xu, J.; Wu, Y.; Xu, H.; Rao, A.; Liu, X. Photon Upconversion Through Triplet Exciton-Mediated Energy Relay. *Nat. Commun.* **2021**, *12* (1), 3704.
(39) Zhang, J.-X.; Chan, W.-L.; Xie, C.; Zhou, Y.; Chau, H.-F.; Maity, P.; Harrison, G. T.; Amassian, A.; Mohammed, O. F.; Tanner, P. A.; Wong, W.-K.; Wong, K.-L. Impressive Near-Infrared Brightness and Singlet Oxygen Generation from Strategic Lanthanide−Porphyrin Double-Decker Complexes in Aqueous Solution. *Light Sci. Appl.* **2019**, *8* (1), 46.
(40) Chong, B. S. K.; Moore, E. G. Quantitative Sensitization Efficiencies in NIR-Emissive Homoleptic Ln(III) Complexes Using 2-(5-Methylpyridin-2-yl)-8-hydroxyquinoline. *Inorg. Chem.* **2018**, *57* (22), 14062−14072.
(41) Zhu, M.; Zhang, H.; Ran, G.; Mangel, D. N.; Yao, Y.; Zhang, R.; Tan, J.; Zhang, W.; Song, J.; Sessler, J. L.; Zhang, J.-L. Metal Modulation: An Easy-to-Implement Tactic for Tuning Lanthanide Phototheranostics. *J. Am. Chem. Soc.* **2021**, *143* (19), 7541−7552.
(42) Ha-Thi, M.-H.; Delaire, J. A.; Michelet, V.; Leray, I. Sensitized Emission of Luminescent Lanthanide Complexes Based on a Phosphane Oxide Derivative. *J. Phys. Chem. A* **2010**, *114* (9), 3264−3269.
(43) Thor, W.; Kai, H.-Y.; Zhang, Y.; Wong, K.-L.; Tanner, P. A. Thermally Activated Photophysical Processes of Organolanthanide Complexes in Solution. *J. Phys. Chem. Lett.* **2022**, *13* (21), 4800−4806.
(44) Tanner, P. A.; Thor, W.; Zhang, Y.; Wong, K.-L. Energy Transfer Mechanism and Quantitative Modeling of Rate from an Antenna to a Lanthanide Ion. *J. Phys. Chem. A* **2022**, *126* (41), 7418−7431.
(45) Freidzon, A. Y.; Scherbinin, A. V.; Bagaturyants, A. A.; Alfimov, M. V. Ab Initio Study of Phosphorescent Emitters Based on Rare-Earth Complexes with Organic Ligands for Organic Electroluminescent Devices. *J. Phys. Chem. A* **2011**, *115* (18), 4565−4573.
(46) Cheung, T.-L.; Tam, L. K. B.; Tam, W.-S.; Zhang, L.; Kai, H.-Y.; Thor, W.; Wu, Y.; Lam, P.-L.; Yeung, Y.-H.; Xie, C.; Chau, H.-F.; Lo, W.-S.; Zhang, T.; Wong, K.-L. Facile Peptide Macrocyclization and Multifunctionalization *via* Cyclen Installation. *Small Methods* **2024**, No. 2400006.

https://doi.org/10.1021/jacsau.4c00468
JACS Au 2024, 4, 3813−3822

(47) Cieslikiewicz-Bouet, M.; Eliseeva, S. V.; Aucagne, V.; Delmas, A. F.; Gillaizeau, I.; Petoud, S. Near-Infrared Emitting Lanthanide(III) Complexes as Prototypes of Optical Imaging Agents with Peptide Targeting Ability: A Methodological Approach. *RSC Adv.* **2019**, *9* (3), 1747−1751.
(48) Choi, J.-H.; Fremy, G.; Charnay, T.; Fayad, N.; Pécaut, J.; Erbek, S.; Hildebrandt, N.; Martel-Frachet, V.; Grichine, A.; Sénèque, O. Luminescent Peptide/Lanthanide(III) Complex Conjugates with Push−Pull Antennas: Application to One- and Two-Photon Microscopy Imaging. *Inorg. Chem.* **2022**, *61* (50), 20674−20689.
(49) Stanimirov, S. S.; Trifonov, A. A.; Buchvarov, I. C. Discovering of the L Ligand Impact on Luminescence Enhancement of Eu(Dibenzoylmethane)$_3$.L$_x$ Complexes Employing Transient Absorption Spectroscopy. *Spectrochim. Acta A Mol. Biomol. Spectrosc.* **2021**, *258*, No. 119832.
(50) Parker, D.; Fradgley, J. D.; Wong, K.-L. The Design of Responsive Luminescent Lanthanide Probes and Sensors. *Chem. Soc. Rev.* **2021**, *50* (14), 8193−8213.
(51) van Stokkum, I. H. M.; Larsen, D. S.; van Grondelle, R. Global and Target Analysis of Time-Resolved Spectra. *Biochimica et Biochim. Biophys. Acta - Bioenergetics* **2004**, *1657* (2), 82−104.
(52) Han, S.; Deng, R.; Gu, Q.; Ni, L.; Huynh, U.; Zhang, J.; Yi, Z.; Zhao, B.; Tamura, H.; Pershin, A.; Xu, H.; Huang, Z.; Ahmad, S.; Abdi-Jalebi, M.; Sadhanala, A.; Tang, M. L.; Bakulin, A.; Beljonne, D.; Liu, X.; Rao, A. Lanthanide-Doped Inorganic Nanoparticles Turn Molecular Triplet Excitons Bright. *Nature* **2020**, *587* (7835), 594−599.
(53) Abbas, Z.; Dasari, S.; Beltrán-Leiva, M. J.; Cantero-López, P.; Páez-Hernández, D.; Arratia-Pérez, R.; Butcher, R. J.; Patra, A. K. Luminescent Europium(III) and Terbium(III) Complexes of β-Diketonate and Substituted Terpyridine Ligands: Synthesis, Crystal Structures and Elucidation of Energy Transfer Pathways. *New J. Chem.* **2019**, *43* (38), 15139−15152.
(54) Riseberg, L. A.; Moos, H. W. Multiphonon Orbit-Lattice Relaxation of Excited States of Rare-Earth Ions in Crystals. *Phys. Rev.* **1968**, *174* (2), 429−438.
(55) Wolf, E. *Progress in Optics*, Vol. *XIV*; North Holland, 1976.
(56) Softley, C. A.; Bostock, M. J.; Popowicz, G. M.; Sattler, M. Paramagnetic NMR in Drug Discovery. *J. Biomol. NMR* **2020**, *74* (6), 287−309.
(57) Faustino, W. M.; Nunes, L. A.; Terra, I. A. A.; Felinto, M. C. F. C.; Brito, H. F.; Malta, O. L. Measurement and Model Calculation of the Temperature Dependence of Ligand-to-Metal Energy Transfer Rates in Lanthanide Complexes. *J. Lumin.* **2013**, *137*, 269−273.
(58) Moore, E. G.; Grilj, J.; Vauthey, E.; Ceroni, P. A Comparison of Sensitized Ln(III) Emission Using Pyridine- and Pyrazine-2,6-dicarboxylates − Part II. *Dalton Trans.* **2013**, *42* (6), 2075−2083.
(59) Werts, M. H. V.; Verhoeven, J. W.; Hofstraat, J. W. Efficient Visible Light Sensitisation of Water-Soluble Near-Infrared Luminescent Lanthanide Complexes. *J. Chem. Soc., Perkin Trans. 2* **2000**, No. 3, 433−439.
(60) Cavalli, E.; Ruggieri, S.; Mizzoni, S.; Nardon, C.; Bettinelli, M.; Piccinelli, F. NIR-Emission from Yb(III)- and Nd(III)-Based Complexes in the Solid State Sensitized by a Ligand System Absorbing in a Broad UV and Visible Spectral Window. *Results Chem.* **2022**, *4*, No. 100388.
(61) Kaur, G.; Dwivedi, Y.; Rai, S. B. Study of Enhanced Red Emission from Sm(Sal)$_3$Phen Ternary Complexes in Polyvinyl Alcohol Film. *Opt. Commun.* **2010**, *283* (18), 3441−3447.
(62) Ilichev, V. A.; Silantyeva, L. I.; Yablonskiy, A. N.; Andreev, B. A.; Rumyantcev, R. V.; Fukin, G. K.; Bochkarev, M. N. Synthesis, Structure and Long-Lived NIR Luminescence of Lanthanide Ate Complexes with Perfluorinated 2-Mercaptobenzothiazole. *Dalton Trans.* **2019**, *48* (3), 1060−1066.
(63) Baek, N. S.; Nah, M. K.; Kim, Y. H.; Kim, H. K. Ln(III)-Cored Complexes Based on 2-Thenoyltrifluoroacetone Ligand for Near Infrared Emission: Energy Transfer Pathway and Transient Absorption Behavior. *J. Lumin.* **2007**, *127* (2), 707−712.
(64) Klink, S. I.; Grave, L.; Reinhoudt, D. N.; van Veggel, F. C. J. M.; Werts, M. H. V.; Geurts, F. A. J.; Hofstraat, J. W. A Systematic Study of the Photophysical Processes in Polydentate Triphenylene-Functionalized Eu^{3+}, Tb^{3+}, Nd^{3+}, Yb^{3+}, and Er^{3+} Complexes. *J. Phys. Chem. A* **2000**, *104* (23), 5457−5468.
(65) Meng, M.; Bai, M.; Da, Z.; Cui, Y.; Li, B.; Pan, J. Selective Recognition of Salicylic Acid Employing New Fluorescent Imprinted Membrane Functionalized with Poly(amidoamine) (PAMAM)-Encapsulated Eu(TTA)$_3$phen. *J. Lumin.* **2019**, *208*, 24−32.
(66) Zhang, Y.; Thor, W.; Wong, K.-L.; Tanner, P. A. Determination of Triplet State Energy and the Absorption Spectrum for a Lanthanide Complex. *J. Phys. Chem. C* **2021**, *125* (13), 7022−7033.
(67) Li, H.; Lan, R.; Chan, C.-F.; Bao, G.; Xie, C.; Chu, P.-H.; Tai, W. C. S.; Zha, S.; Zhang, J.-X.; Wong, K.-L. A Luminescent Lanthanide Approach Towards Direct Visualization of Primary Cilia in Living Cells. *Chem. Commun.* **2017**, *53* (52), 7084−7087.
(68) Mullen, K. M.; van Stokkum, I. H. M. TIMP: An R Package for Modeling Multi-way Spectroscopic Measurements. *J. Stat. Softw.* **2007**, *18* (3), 1−46.
(69) Snellenburg, J. J.; Laptenok, S.; Seger, R.; Mullen, K. M.; van Stokkum, I. H. M. Glotaran: A Java-Based Graphical User Interface for the R Package TIMP. *J. Stat. Softw.* **2012**, *49* (3), 1−22.
(70) Frisch, M. J.; Trucks, G. W.; Schlegel, H. B.; Scuseria, G. E.; Robb, M. A.; Cheeseman, J. R.; Scalmani, G.; Barone, V.; Petersson, G. A.; Nakatsuji, H.; Li, X.; Caricato, M.; Marenich, A. V.; Bloino, J.; Janesko, B. G.; Gomperts, R.; Mennucci, B.; Hratchian, H. P.; Ortiz, J. V.; Izmaylov, A. F.; Sonnenberg, J. L.; Williams; Ding, F.; Lipparini, F.; Egidi, F.; Goings, J.; Peng, B.; Petrone, A.; Henderson, T.; Ranasinghe, D.; Zakrzewski, V. G.; Gao, J.; Rega, N.; Zheng, G.; Liang, W.; Hada, M.; Ehara, M.; Toyota, K.; Fukuda, R.; Hasegawa, J.; Ishida, M.; Nakajima, T.; Honda, Y.; Kitao, O.; Nakai, H.; Vreven, T.; Throssell, K.; Montgomery, J. A., Jr.; Peralta, J. E.; Ogliaro, F.; Bearpark, M. J.; Heyd, J. J.; Brothers, E. N.; Kudin, K. N.; Staroverov, V. N.; Keith, T. A.; Kobayashi, R.; Normand, J.; Raghavachari, K.; Rendell, A. P.; Burant, J. C.; Iyengar, S. S.; Tomasi, J.; Cossi, M.; Millam, J. M.; Klene, M.; Adamo, C.; Cammi, R.; Ochterski, J. W.; Martin, R. L.; Morokuma, K.; Farkas, O.; Foresman, J. B.; Fox, D. J. *Gaussian 16* Rev. C.01; Gaussian Inc.: Wallingford CT, 2016.
(71) Hanwell, M. D.; Curtis, D. E.; Lonie, D. C.; Vandermeersch, T.; Zurek, E.; Hutchison, G. R. Avogadro: An Advanced Semantic Chemical Editor, Visualization, and Analysis Platform. *J. Cheminf.* **2012**, *4* (1), 17.
(72) Neese, F. The ORCA Program System. *WIREs Comput. Mol. Sci.* **2012**, *2* (1), 73−78.
(73) Neese, F. Software Update: the ORCA Program System, Version 4.0. *WIREs Comput. Mol. Sci.* **2018**, *8* (1), No. e1327.
(74) Andrae, D.; Häußermann, U.; Dolg, M.; Stoll, H.; Preuß, H. Energy-Adjusted ab initio Pseudopotentials for the Second and Third Row Transition Elements. *Theor. Chim. Acta* **1990**, *77* (2), 123−141.
(75) Dolg, M.; Stoll, H.; Savin, A.; Preuss, H. Energy-Adjusted Pseudopotentials for the Rare Earth Elements. *Theor. Chim. Acta* **1989**, *75* (3), 173−194.
(76) Cao, X.; Dolg, M. Segmented Contraction Scheme for Small-Core Lanthanide Pseudopotential Basis Sets. *J. Mol. Struct. Theochem* **2002**, *581* (1), 139−147.
(77) Pettersen, E. F.; Goddard, T. D.; Huang, C. C.; Couch, G. S.; Greenblatt, D. M.; Meng, E. C.; Ferrin, T. E. UCSF Chimera − A Visualization System for Exploratory Research and Analysis. *J. Comput. Chem.* **2004**, *25* (13), 1605−1612.

https://doi.org/10.1021/jacsau.4c00468
JACS Au 2024, 4, 3813−3822